ELSEVIER

Contents lists available at ScienceDirect

Extreme Mechanics Letters

journal homepage: www.elsevier.com/locate/eml



Mechanics of bonded sensor layers in soft tubes: Suppressing instability and failure for sensing reliability

Yi Jin^a, Christian A. Zorman^{b,c}, Changyong Chase Cao^{a,b,c,*}

- ^a Department of Mechanical and Aerospace Engineering, Case Western Reserve University, Cleveland, OH 44106, USA
- ^b Department of Electrical, Computer and Systems Engineering, Case Western Reserve University, Cleveland, OH 44106, USA
- ^c Advanced Platform Technology (APT) Center, Louis Stokes Cleveland VA Medical Center, Cleveland, OH 44106, USA

ARTICLE INFO

Keywords: Soft tubes Bonded sensors Ovalization Buckling Sensor failure Measurement fidelity Structural instability

ABSTRACT

Integrating sensors onto thin-walled tubular structures is of paramount importance for the advancement of smart infrastructures and facilities, enabling real-time detection of mechanical states and environmental conditions. This study systematically investigates the mechanics of bonded sensor layers in suppressing bending-induced ovalization, buckling, and failure in soft, thin-walled tubes, with the goal of enhancing sensing reliability. While significant progress has been made in understanding instability phenomena in tubular structures under mechanical loading, a critical gap remains in characterizing how bonded sensor layers influence deformation and failure mechanisms. To address this, a comprehensive parametric analysis—supported by finite element simulations and experimental validation—was conducted to evaluate the effects of four key parameters: length ratio, thickness ratio, wrapped angle, and relative stiffness. The results reveal that optimized configurations-specifically, length ratios exceeding 0.7, thickness ratios above 1.6, moderate wrapped angles (approximately $2\pi/3-4\pi/3$), and relative stiffness greater than 0.03—can suppress ovalization to below 25 % in sensor-covered regions, redistribute deformation to uncovered segments, and trigger complex buckling behaviors involving multiple kinks and secondary instabilities. These thresholds mitigate localized strain concentrations, reduce the risk of sensor layer wrinkling or delamination, and preserve measurement fidelity under operational loading. The findings extend classical instability theories to hyperelastic, multilayered systems and provide practical design guidelines for sensor-integrated tubular structures. Applications include smart pipelines and conduits for structural health monitoring and environmental sensing in next-generation infrastructure systems.

1. Introduction

Smart infrastructures and facilities increasingly rely on integrated sensor technologies for real-time monitoring and enhanced operational efficiency, such as in pipelines, structural components, and environmental systems [1–4]. Thin-walled tubular structures equipped with bonded sensor layers represent a critical advancement in these domains, enabling the detection of mechanical states and environmental conditions [4]. These smart tubes are designed to adapt to complex environments while providing data on parameters like internal pressure or structural integrity. Consequently, the system can be modeled as a thin-walled tube integrated with bonded sensor layers [5,6]. In operational scenarios, these tubular structures are particularly susceptible to bending loads, which induce ovalization and buckling [7]. Ovalization denotes the deformation of the tube's circular cross-section into an oval

or elliptical shape during bending [8]. Excessive ovalization may undermine the tube's structural integrity, create localized stress concentrations, and promote sensor layer failure modes such as wrinkling or delamination, thereby compromising sensing fidelity [9–11]. Furthermore, the interaction between ovalization and wall flattening can result in distinct loading and unloading paths, generating hysteresis that requires accurate capture by the sensor.

The integration of sensor layers in tubular structures holds significant promise across diverse applications, enhancing reliability and functionality under deformation [4]. In smart infrastructures, these configurations facilitate pipeline inspection for leak detection and integrity assessment, structural health monitoring in bridges and buildings to prevent failures, and environmental sensing in water distribution systems for contamination detection. Similarly, in soft robotics [12–14], they enable minimally invasive medical devices for precise

^{*} Corresponding author at: Department of Mechanical and Aerospace Engineering, Case Western Reserve University, Cleveland, OH 44106, USA. *E-mail address:* ccao@case.edu (C.C. Cao).

navigation and force feedback [15,16], agricultural grippers for delicate harvesting tasks [17,18], and exploration robots for subsurface or confined-space operations [19]. By addressing deformation challenges in these scenarios, such as ensuring sensor durability during bending, the technology supports broader impacts including improved safety, efficiency, and adaptability in both infrastructural and robotic systems.

Extensive research has investigated ovalization and buckling in tubes without bonded sensor layers or rigid reinforcements, utilizing analytical [20-22], numerical [23-26], and experimental [27,28] approaches. A significant portion of analytical studies extends Brazier's methodology [8], linking bending curvature to cross-sectional instability. Wilkes enhanced Brazier's model by developing an analytical framework that describes the combined effects of bending, pressure, and axial loads on ovalization and collapse in cylindrical tubes [29]. Zhang and Yu examined ovalization in tubes with arbitrary cross-sections, establishing the full moment-curvature relationship [30]. Their analysis demonstrated that flattening increases nonlinearly with longitudinal curvature. In cases with complex boundary conditions and nonlinear materials, approximate solutions or finite element analyses are typically employed [31,32]. Despite progress in understanding thin-walled tube instability under various loads, a substantial knowledge gap remains concerning the impact of a bonded sensor layer on deformation and instability in

To bridge this gap, this study performs a parametric analysis of the bonded sensor layer's geometric and material properties on ovalization and buckling in thin-walled tubes through finite element analysis and experimental validation. As shown in Fig. 1(a), the simulations feature partial bonding of a sensor layer around the central portion of a thin-walled tube, bent by moments applied at its ends. During the process, the tube's cross-section experiences ovalization and flattening, potentially leading to one or two kinks, as illustrated in Fig. 1(b). Ovality is the measure of the ovalization of a cylindrical object's cross-section from a perfect circle, typically expressed as the difference between its maximum and minimum diameters divided by the nominal diameter. Following standard convention, ovalization is expressed as:

$$\eta = rac{D_{ ext{max}} - D_{ ext{min}}}{D_{ ext{max}} + D_{ ext{min}}} imes 100\%$$

where η is the ovality of the tube cross-section during bending, and $D_{\rm max}$ and $D_{\rm min}$ are the major and minor outer diameters, respectively. This

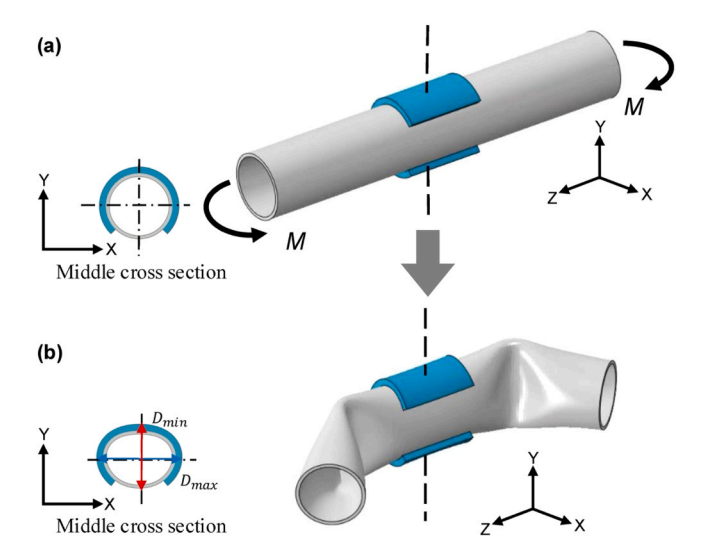


Fig. 1. Schematic of a soft, thin-walled tube under bending with a bonded extensible layer at the midsection. (a) The tube is partially wrapped by an extensible layer and subjected to a bending moment at both ends. (b) During bending, the tube undergoes cross-sectional ovalization and may buckle; the extensible layer constrains ovalization and influences the buckling behavior.

study covers three geometric parameters of the sensor layer—length, thickness, and wrapped angle—as well as the relative stiffness between the tube and the layer. The findings are detailed in the following sections.

The organization of this paper is as follows: Section 2 presents the computational and experimental approach used in the study. Section 3 discusses the bending behavior of a baseline tube without a bonded sensor layer. Section 4 examines the critical factors influencing tube ovalization and buckling—specifically, length ratio, thickness ratio, wrapped angle, and relative stiffness—and analyze their effects on bending behavior as well as strategies to prevent failure and ensure the reliability of integrated sensors. Finally, Section 5 provides concluding insights and suggestions for future research.

2. Computational and experimental approach

To investigate the influence of bonded sensor layers on tube deformation, finite element (FE) simulations were implemented using the commercial software AbaqusTM. Computer-aided design (CAD) models of tubes integrated with sensor layers of varying geometric parameters were generated in SolidWorksTM and imported into AbaqusTM. A neo-Hookean hyperelastic model was assigned to the tube material, with coefficients $C_{10}=1$ MPa and $D_1=0.01$ MPa⁻¹, reflecting the soft material properties. Solid elements (C3D10H) were employed for meshing the tube. For the sensor layer, a similar neo-Hookean model was applied, with coefficients $C_{10}=0.02\ MPa$ and $D_1=0.01\ MPa^{-1}$ for geometric parameter studies, while varying these for relative stiffness analyses. The layer was also meshed with C3D10H elements. During simulations, the longitudinal motion at the tube's mid-plane was constrained, and displacement loadings were applied at the ends to achieve specified bending angles. Moment and angle data were extracted from the tube ends for analysis. Mesh convergence was verified by refining element sizes until ovality variations were below 1 %, ensuring computational accuracy. Failure criteria for the sensor layer were incorporated by monitoring maximum principal strains, with thresholds set at 150 % to identify potential wrinkling or delamination risks, based on material

Complementing the simulations, experiments were conducted to validate deformation behaviors. Tubes were fabricated using a digital light processing (DLP) resin printer (Photon Mono M7, Anycubic™) with a commercial UV-curable flexible resin (F69, RESIONETM). Postprinting, specimens were cured under 405 nm UV light for 30 min, followed by oven curing at 60 °C for 1 h, yielding a Young's modulus of approximately 10 MPa. VHB tapes (4905 and 4910, 3MTM) with thicknesses of 0.5 mm and 1 mm, and an assumed Young's modulus of 0.2 MPa, served as sensor layer analogs. A custom bending test apparatus was designed, comprising a rigid base plate with a semicircular track and two movable sliders (see Supporting information, Fig. S2). Tube ends were clamped to the sliders to preserve cross-sectional shape during bending, with sliders moving along the track for controlled deformation. Longitudinal motion at mid-span was restricted using a thin thread. A camera captured configurations at specified angles for ovality quantification via image analysis, with measurements showing agreement within 10 % of FE predictions, accounting for material variability.

3. Baseline behavior of the tube under bending loads

Initial simulations investigated a tube without a bonded sensor layer to establish baseline insights into geometric influences on ovalization and buckling. Given the focus on soft materials, a neo-Hookean model was employed, as described in Section 2. As shown in Fig. 2(a), the tube bends about its mid-plane by an angle θ . During bending, both end cross-sections were assumed to remain constant, and displacement-controlled loading was applied to achieve the target angle. The tube had an outer diameter $D=20\,\mathrm{mm}$ and wall thickness t, defining the

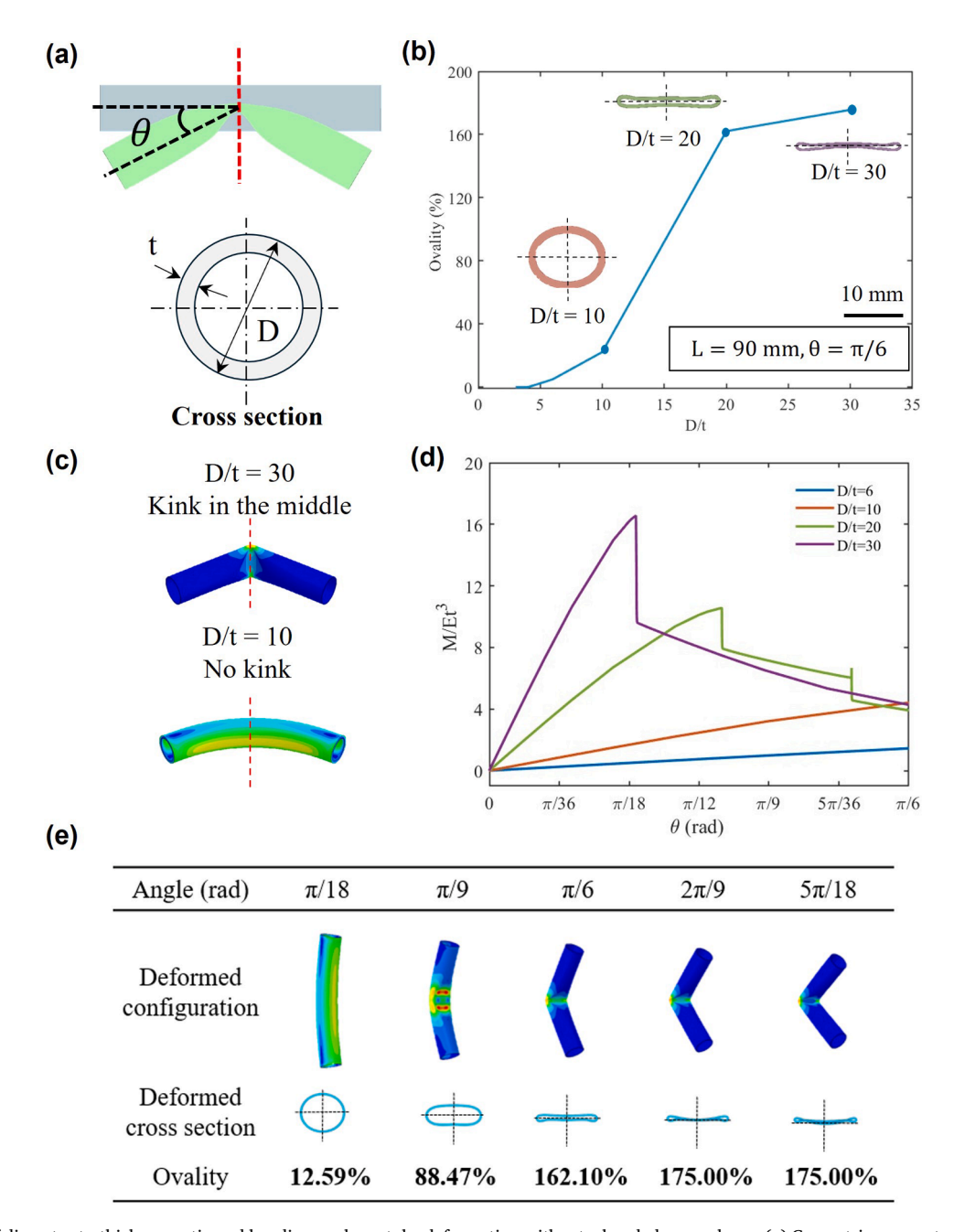


Fig. 2. Influence of diameter-to-thickness ratio and bending angle on tube deformation without a bonded sensor layer. (a) Geometric parameters of the tube. (b) FEA results showing ovality at a bending angle of $\pi/6$ for varying diameter-to-thickness ratios. (c) Configurations of bent tubes at different diameter-to-thickness ratios. (d) FEA results of normalized moment—angle curves for tubes with different diameter-to-thickness ratios. (e) Effect of increasing bending angle on tube ovality and deformation configuration for a fixed ratio.

diameter-to-thickness ratio D/t (examined values: 6, 10, 20, 30). Tube length was fixed at L = 100 mm, with bending up to $\theta=\pi/6$. Fig. 2(b) presents the maximum ovality at $\theta=\pi/6$ for different D/t ratios. Ovalization increased with D/t, with a distinct mid-plane kink forming at D/t > 20. For D/t < 10, the cross-sections remained nearly circular, as shown in Fig. 2(c). Thinner walls facilitated more significant ovalization, which may pose challenges for maintaining structural integrity during sensor layer integration in smart infrastructure applications.

Normalized bending moment curves, $M/(Et^3)$, are plotted against θ in Fig. 2(d), where E is the Young's modulus. Buckling was observed at $\theta \approx \pi/12$ for D/t = 30 (critical normalized moment \approx 17), and at $\theta \approx \pi/9$ for D/t = 20 (critical normalized moment \approx 12). Tubes with D/t < 10 remained stable up to $\theta = \pi/6$. These trends are consistent with Brazier theory [8], validating its relevance to soft materials, although

the neo-Hookean model revealed stronger post-buckling softening than predicted by linear elasticity. Based on these observations, a tube with D/t=20 was selected for further analysis. Fig. 2(e) explores the effect of bending angle from $\theta=0$ to $\pi/2.$ Ovality exceeded 25 % beyond $\pi/6,$ accompanied by mid-plane kinking, and reached a maximum at $\pi/3$ with inner surface contact. Ovality generally increased with bending angle, reinforcing the importance of sensor layer bonding to suppress deformation and maintain sensing accuracy under operational loading. These results establish a critical bifurcation point, where localized strain energy triggers instability, consistent with buckling behaviors in elasto-active soft structures.

4. Bending behavior of the tube with bonded sensor layer

This section investigates the influence of a bonded sensor layer on the deformation and buckling behavior of a soft, thin-walled tube, building on the computational and experimental approach described in Section 2. As illustrated in Fig. 3(a), the tube has length L, thickness t, and shear modulus μ_t . The sensor layer is bonded at the tube's midsection, with length 1, thickness t₁, and shear modulus μ_t . The wrapped angle α defines the positive central angle spanned by the layer. Four normalized parameters were analyzed to isolate geometric and material effects: length ratio 1/L, thickness ratio t_1/t , wrapped angle α .

and relative stiffness μ_1/μ_t .

Three distinct types of normalized moment-bending angle curves characterize the bending response of tubes with bonded sensor layers (Supporting information, Fig. S3). The first type (Fig. S3(a)) exhibits three regions: elastic, ovalization, and post-buckling, with two critical points. From $\theta=0$ to $\pi/18$ radians, the moment (M/Et^3) increases linearly, indicating an elastic response with a circular cross-section. Between $\pi/18$ and $\pi/9$, nonlinearity emerges as ovalization begins, increasing local stresses that could risk sensor layer wrinkling. At $\theta=\pi/9$, the curve peaks (critical moment ~ 14), followed by a sharp drop, signaling local buckling with a mid-plane kink formation. Beyond

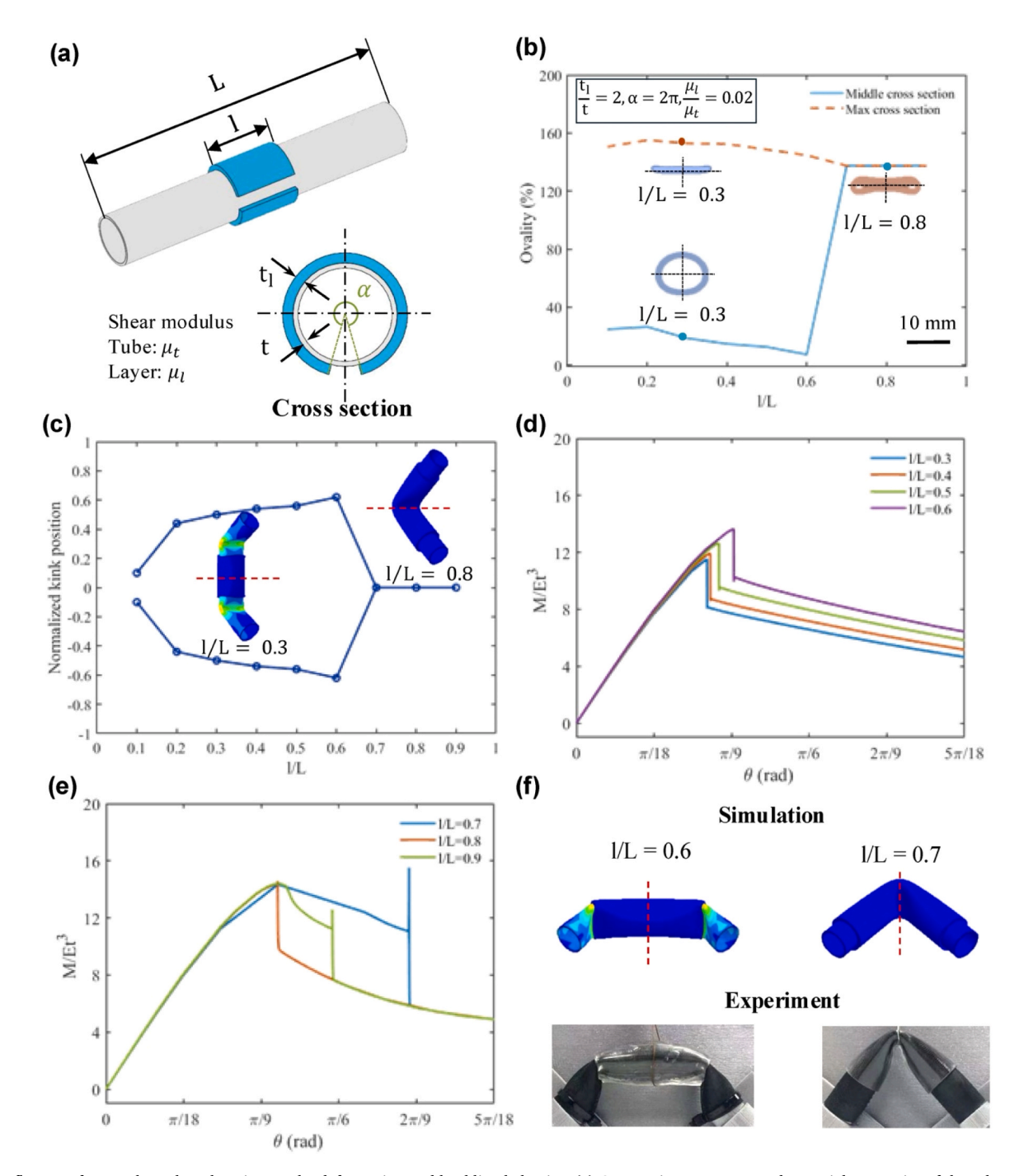


Fig. 3. Influence of sensor layer length ratio on tube deformation and buckling behavior. (a) Geometric parameters and material properties of the tube and bonded layer. (b) FEA results of ovality at a bending angle of $5\pi/18$ for varying length ratios. (c) Normalized kink position relative to the tube centerline. (d–e) FEA results of normalized moment–bending angle curves for different length ratios: (d) 1/L = 0.3–0.6; (e) 1/L = 0.7–0.9. (f) Comparison of FEA and experimental deformation during bending for tubes with different sensor layer lengths.

this, the moment declines, reflecting reduced load-carrying capacity and potential layer failure due to stress concentrations. This behavior underscores the need for layer optimization to maintain sensing fidelity.

The second type (Fig. S3(b)) features four regions: elastic, ovalization, post-buckling, and post-collapse, with two instability points. After an initial elastic phase, ovalization induces nonlinearity, with the critical moment (~ 14) at $\theta=\pi/9$. Post-buckling, the moment decreases gradually as small wrinkles form on the compressive side, reducing stiffness but retaining some load capacity. At $\theta=13\pi/60$, a slight moment increase precedes a sharp drop, indicating snap-through instability where wrinkles coalesce into larger folds, temporarily enhancing stiffness before collapse. Experiments confirm these patterns, showing that strategic layer design mitigates wrinkling, preserving structural and sensing reliability in smart infrastructure applications.

The third type (Fig. S3(c)) mirrors the second but exhibits post-snapthrough fluctuations, reflecting dynamic load redistribution. After initial elastic deformation and ovalization, local buckling occurs, followed by snap-through at $\theta \approx 13\pi/60$. Subsequent oscillations arise from kink migration along the compressive surface, as wrinkles coalesce into larger folds seeking stable configurations. This migration, observed in both simulations and experiments, dissipates energy incrementally, delaying complete collapse. The dynamic behavior highlights complex tube-layer interactions, where optimized parameters can reduce layer failure risks (e.g., delamination) and ensure consistent sensing performance under large deformations. These curves demonstrate that bonded sensor layers significantly influence tube mechanics, with implications for preventing failure modes and maintaining sensing reliability. Subsequent subsections explore specific parameter effects to optimize these outcomes.

4.1. Effects of length ratio in bonded sensor layers

This section investigates how the length ratio 1/L affects ovalization and buckling, with other parameters fixed at $t_1/t=2$, $\alpha=2\pi$, and $\mu_l/\mu_t=0.2$. The tube is bent to a constant angle of $5\pi/18$ radians. Fig. 3 (b) presents the finite element analysis (FEA) results of ovality for varying length ratios. When 1/L<0.7, the tube collapses on both sides of the sensor layer, exhibiting extreme ovality (up to 150 %), while the mid-plane remains nearly circular (ovality <40 %). This is due to the lower stiffness of the uncovered regions, which reach their critical moments before the covered region. As 1/L increases, ovality at both the middle and maximum planes decreases. For $1/L \ge 0.7$, collapse occurs in the mid-plane itself, with an ovality of 137.43 %, indicating nearly simultaneous instability in both covered and uncovered regions.

Fig. 3(c) shows the normalized kink position versus length ratio, calculated as $\pm a/(L/2)$, where a is the distance of the kink from the midplane. For 1/L<0.7, two symmetric kinks appear away from the center. As the length ratio increases, these kinks migrate outward. At $1/L\geq0.7$, only one central kink forms, indicating a shift in the dominant buckling location. The normalized moment–bending angle curve for 1/L<0.7 is presented in Fig. 3(d). The moment rises linearly, then drops sharply at the critical point, followed by a gradual decline. As the length ratio increases, the critical moment rises and occurs later in the deformation process, consistent with delayed instability. For example, the critical moment for 1/L=0.6 is 13.62. Post-buckling behavior is similar across these cases, as buckling occurs in the identical uncovered region.

For $1/L \ge 0.7$, Fig. 3(e) shows that the normalized moment also rises linearly, followed by varied post-buckling responses. At 1/L = 0.8, the moment drops abruptly and then decreases gradually. At 1/L = 0.7 and 0.9, the moment first decreases gradually, accompanied by surface wrinkling and stiffness loss. This is followed by a sharp fluctuation—a rise and drop—reflecting a second buckling event where initial wrinkles coalesce into larger features, momentarily increasing structural stiffness before a final decline. All three cases share the same critical moment (= 14.21) and final deformation pattern, suggesting that beyond a

threshold ($1/L \ge 0.7$), the length ratio no longer influences the critical moment or post-buckling path. Experimental validation of the deformation profiles for 1/L = 0.6 and 0.7 is provided in Fig. 3(f).

These findings reveal a stiffness-gradient-induced bifurcation mechanism, where extending the sensor layer redistributes strain energy, delays the onset of buckling, and suppresses catastrophic midplane collapse. The results align with nonlinear finite element models of pre-stressed tubular systems, extending Brazier's classical theory by incorporating hyperelastic effects that intensify secondary buckling through wrinkle coalescence. In smart infrastructure applications—such as pipeline health monitoring under seismic or wind-induced bending—optimized sensor layer length ratios (1/L > 0.7) improve structural stability and sensing reliability, reducing the risk of delamination. However, the assumption of perfect bonding may oversimplify realworld conditions. Interfacial shear lags or imperfect adhesion could shift kink locations and deformation modes. Future studies should consider cohesive zone models [33] or introduce internal pressure loading to explore more realistic scenarios.

4.2. Effects of thickness ratio in bonded sensor layers

This section explores how the thickness of a bonded sensor layer influences ovalization and buckling in a soft tubular structure. The sensor layer's length ratio and wrapped angle are held constant at 1/L=0.2 and $\alpha=\pi$, respectively. The thickness ratio t_1/t is varied from 0.4 to 2.8, and all simulations are conducted under a fixed bending angle of $\theta=5\pi/18$ radians. Figs. 4(a) and 4(b) present FEM results for ovality and normalized kink position at the specified bending angle. For a thin layer ($t_1/t=0.4$), the tube exhibits a single central kink, with ovality reaching ~ 160 %. However, once the thickness ratio exceeds 0.8, the deformation pattern shifts: ovality drops below 40 %, and two distinct kinks form near the edges of the sensor layer. The normalized kink position plot shows that increasing thickness causes the kink locations to migrate toward the mid-span (y=0.5). This trend highlights the role of sensor layer thickness in constraining ovalization and redistributing deformation, thereby preventing localized structural collapse.

Figs. 4(c) and 4(d) exhibit the normalized moment-bending angle relationships. For $t_l/t < 1.6$, the moment curves resemble those observed for length ratios l/L < 0.7, indicating that thinner layers do not significantly alter critical buckling behavior. Critical moments remain close to those of the uncovered tube. In contrast, for $t_1/t = 1.6$ and 2.0, a second buckling event emerges, characterized by moment fluctuations and surface wrinkling. Tubes with $t_1/t > 1.6$ exhibit consistent deformation behavior, with closely grouped kink positions and converging moment-angle curves in the post-buckling regime. This suggests a saturation effect, where further increases in thickness provide diminishing structural benefit. Experimental validations for three representative cases are provided in Fig. 4(e): (1) single-kink case ($t_l/t = 0.4$), (2) transitional case $(t_1/t = 1.2)$, and (3) dual-kink case $(t_1/t = 2.0)$. Experimental deformation patterns and kink positions show good agreement with the FEA predictions, confirming the model's ability to accurately capture the effects of thickness on buckling behavior.

These results demonstrate a thickness-dependent stabilization mechanism, whereby increased bending stiffness from the sensor layer suppresses hoop strain gradients and delays instability onset. This shifts the dominant buckling mode and improves collapse resistance. The results extend classical Brazier theory by incorporating the role of layered hyperelasticity, which introduces enhanced post-buckling resilience through distributed strain energy dissipation. In practical applications such as structural health monitoring of pipelines or soft infrastructure, optimizing the thickness ratio ($t_l/t > 1.6$) improves the mechanical integrity of the sensor layer, reduces stress concentrations, and minimizes the risk of delamination—enhancing long-term sensing reliability.

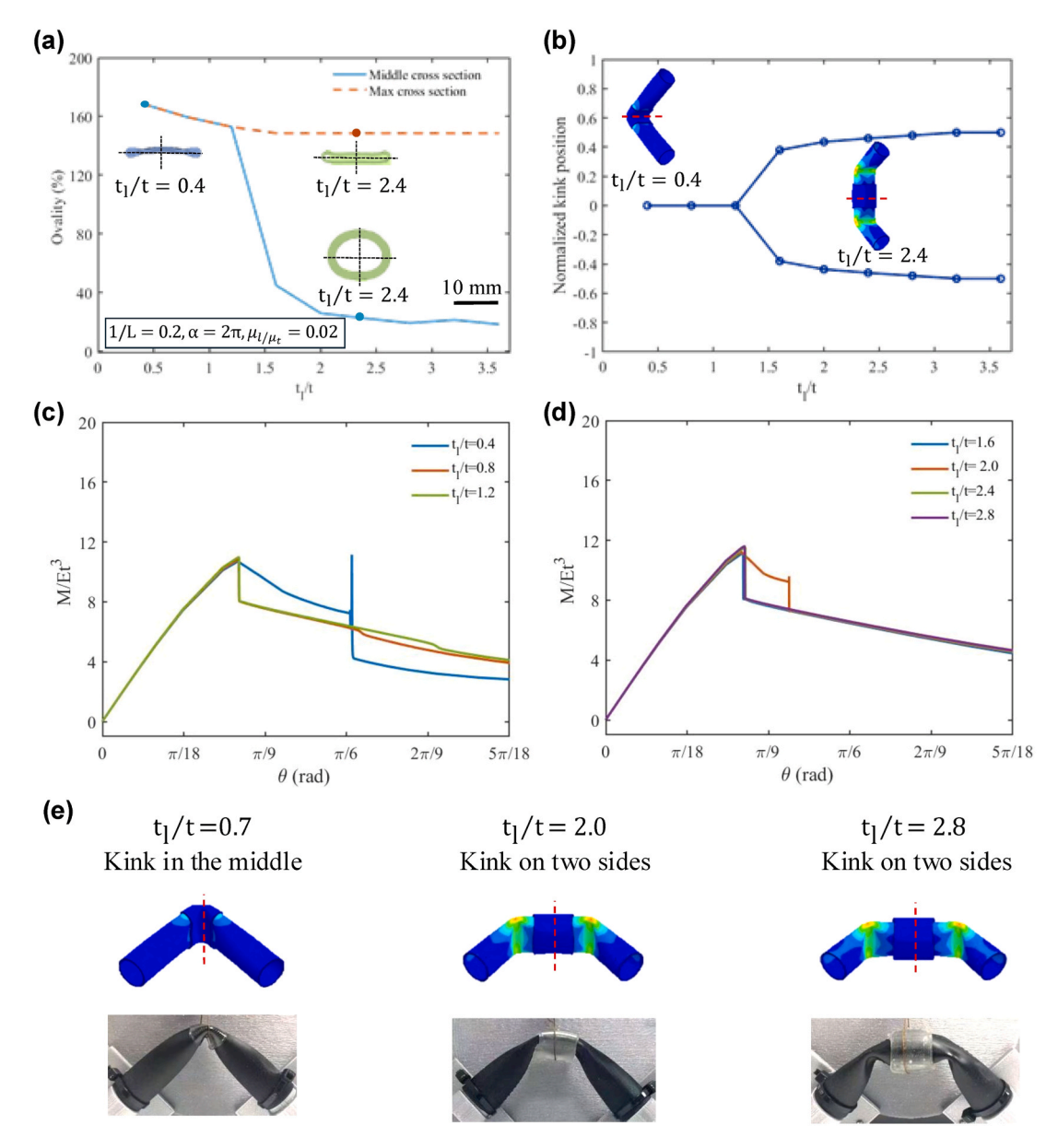


Fig. 4. Influence of sensor layer thickness ratio on ovalization and buckling behavior. (a) FEA results of ovality at a bending angle of $5\pi/18$ for different thickness ratios. (b) Normalized kink position relative to the tube centerline. (c–d) FEA results of normalized moment–bending angle curves for different thickness ratios: (c) $t_1/t = 0.4$ –1.2; (d) $t_1/t = 1.6$ –2.8. (e) Comparison of FEA and experimental deformation during bending for tubes with varying sensor layer thicknesses.

4.3. Effects of wrapped angle in bonded sensor layers

This section investigates how the wrapped angle α of a bonded sensor layer affects ovalization and buckling in soft tubular structures. In practical applications, sensor layers often cover only a portion of the tube circumference, making it essential to understand the influence of partial wrapping. Wrapped angles were varied from $\pi/6$ to 2π in increments of $\pi/6$, while keeping other parameters fixed: 1/L=0.2, $t_1/t=2$, and $\mu_1/\mu_t=0.2$. The sensor layer was positioned on the compressive side of the bent tube. Bending is about symmetric axis (Results for asymmetric conditions are shown in Fig. S4). Fig. 5(a) shows FEA results for ovality across different wrapped angles. Four distinct deformation regimes emerge:

• Small angles $(\pi/6 \le \alpha \le \pi/2)$: A single central kink forms at the mid-plane, with ovality reaching ~ 160 %, indicating collapse in the uncovered region due to insufficient constraint.

- Moderate angles ($\pi/2 < \alpha \le 4\pi/3$): The tube develops two kinks near the edges of the sensor layer, with maximum ovality around 158 % and reduced ovality (< 40 %) at the center, reflecting increased constraint in the covered zone.
- Large angles ($4\pi/3 < \alpha \le 3\pi/2$): The system reverts to a single central kink, likely due to geometric symmetry favoring energy minimization.
- \bullet Very large angles ($\alpha>3\pi/2$): Two kinks reappear, with ovality \sim 160 % and suppressed mid-plane deformation.

This non-monotonic trend reveals that increased coverage initially suppresses mid-plane buckling by shifting instability toward uncovered regions. However, when wrapping approaches half the circumference ($\alpha \approx \pi$), symmetry-induced energy minimization re-establishes a central kink. Further increases in α reinforce stiffness in the covered region, again driving edge-localized buckling.

Fig. 5(b)-(d) present normalized moment-bending angle curves grouped by wrapped angle:

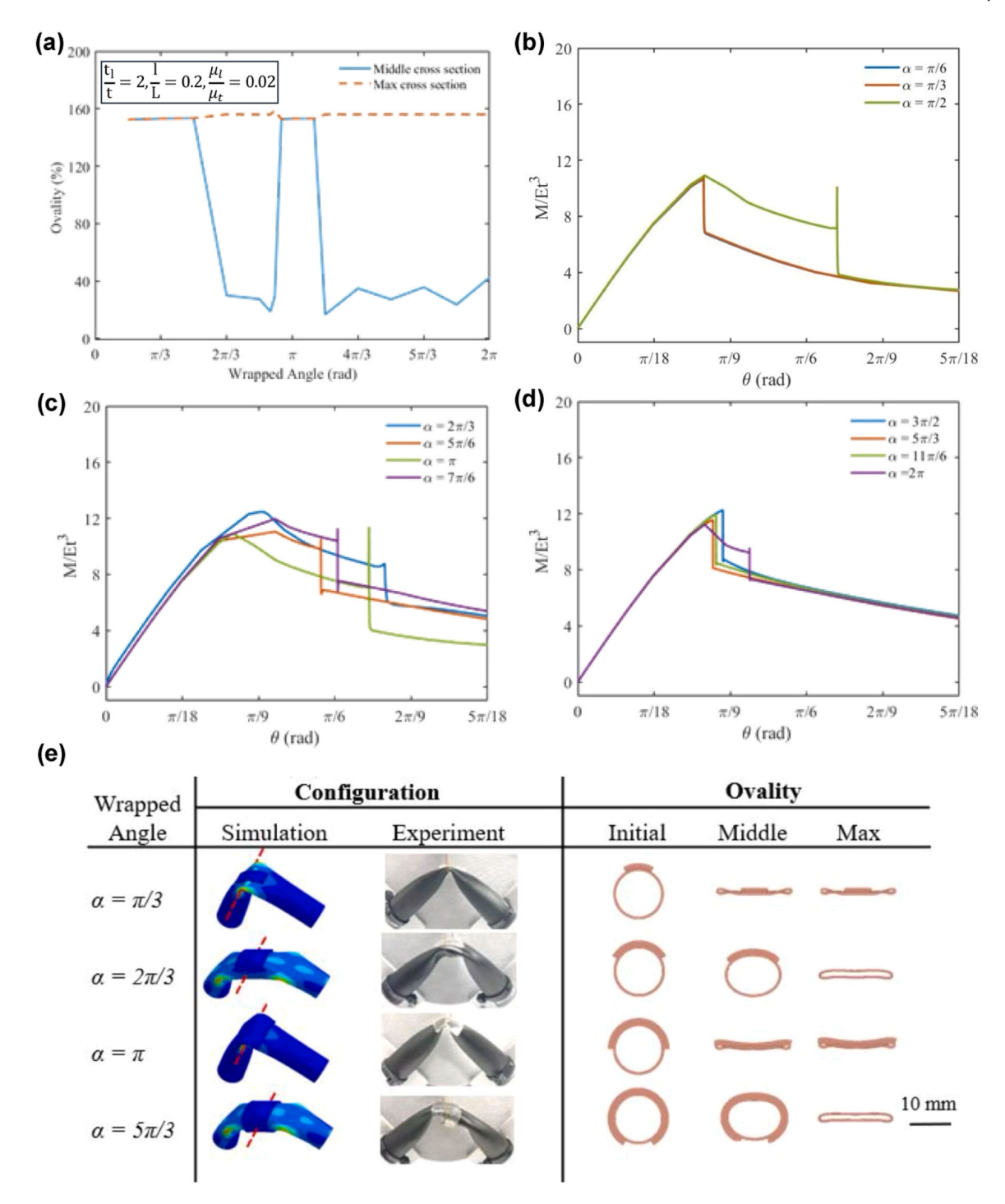


Fig. 5. Influence of wrapped angle of the sensor layer on tube ovalization and buckling behavior. (a) FEA results of ovality at a bending angle of $5\pi/18$ for various wrapped angles. (b–d) FEA results of normalized moment–bending angle curves for different wrapped angle ranges: (b) $\alpha = \pi/6 - \pi/2$; (c) $\alpha = 5\pi/6 - 4\pi/3$; (d) $\alpha = 3\pi/2 - 2\pi$. (e) Comparison of FEA and experimental deformation during bending for tubes with different wrapped angles.

- Small angles ($\pi/6 \le \alpha \le \pi/2$, Fig. 5(b)): The sensor layer provides minimal constraint. Critical moments and post-buckling paths remain similar to the uncovered case.
- Moderate angles $(2\pi/3 \le \alpha \le 7\pi/6$, Fig. 5(c)): Tubes exhibit multistage buckling, with variable critical moments and wrinkle formation, indicating transitional behavior.
- Large angles $(3\pi/2 \le \alpha \le 2\pi$, Fig. 5(d)): Buckling localizes to uncovered regions. As α increases, the critical moment decreases, and instability occurs earlier due to increased constraint within the covered zone.

Fig. 5(e) compares experimental results with simulations, including cross-sectional views from FEA. The experimental deformation patterns confirm the simulation predictions, validating both kink location and ovality trends across wrapped angles.

These analyses reveal an asymmetry-driven mode transition mechanism, in which partial wrapping introduces circumferential stiffness gradients that reshape buckling pathways and deformation energy distributions. This builds upon classical Brazier theory by incorporating non-uniform circumferential constraints in hyperelastic tubes. Notably, moderate wrapping angles promote secondary buckling and wrinkle

formation through localized strain amplification, consistent with recent nonlinear analyses of layered or notched soft structures. In the context of smart infrastructure systems—such as flexible pipelines under seismic loading or bridge components under dynamic stress—moderate wrapped angles provide a balance between structural constraint and flexibility. They enable targeted sensor deployment, mitigate wrinkling, and preserve sensing fidelity by preventing excessive ovalization.

4.4. Effects of relative stiffness in bonded sensor layers

This section examines the effect of relative stiffness between the bonded sensor layer and the soft tube on deformation and buckling behavior. The stiffness ratio μ_l/μ_t was varied across 16 combinations in the form $(b\times 10^n|b=1,2,3,4;n=-3,-2,-1,0)$, covering four orders

of magnitude. The corresponding ovality and normalized kink positions are shown in Figs. 6(a) and 6(b). For relative stiffness values less than 0.01, the tube exhibits a single central kink, with minimal influence from the sensor layer on ovalization. At a stiffness ratio of exactly 0.01, two distinct kinks appear near the edges of the layer, reaching a maximum ovality of 175 %, while mid-plane ovality decreases to 59 %. As the stiffness ratio increases beyond 0.01, ovalization at the mid-plane sharply declines, falling below 25 % for $\mu_l/\mu_t > 0.03$, indicating significant constraint from the stiffer layer. However, the uncovered regions still undergo high deformation, with ovalities near 155 %, leading to localized collapse. The kink positions in these uncovered regions shift outward with increasing layer stiffness. Normalized moment–bending angle curves for each stiffness regime are presented in Fig. 6(c)–(f), grouped by order of magnitude:

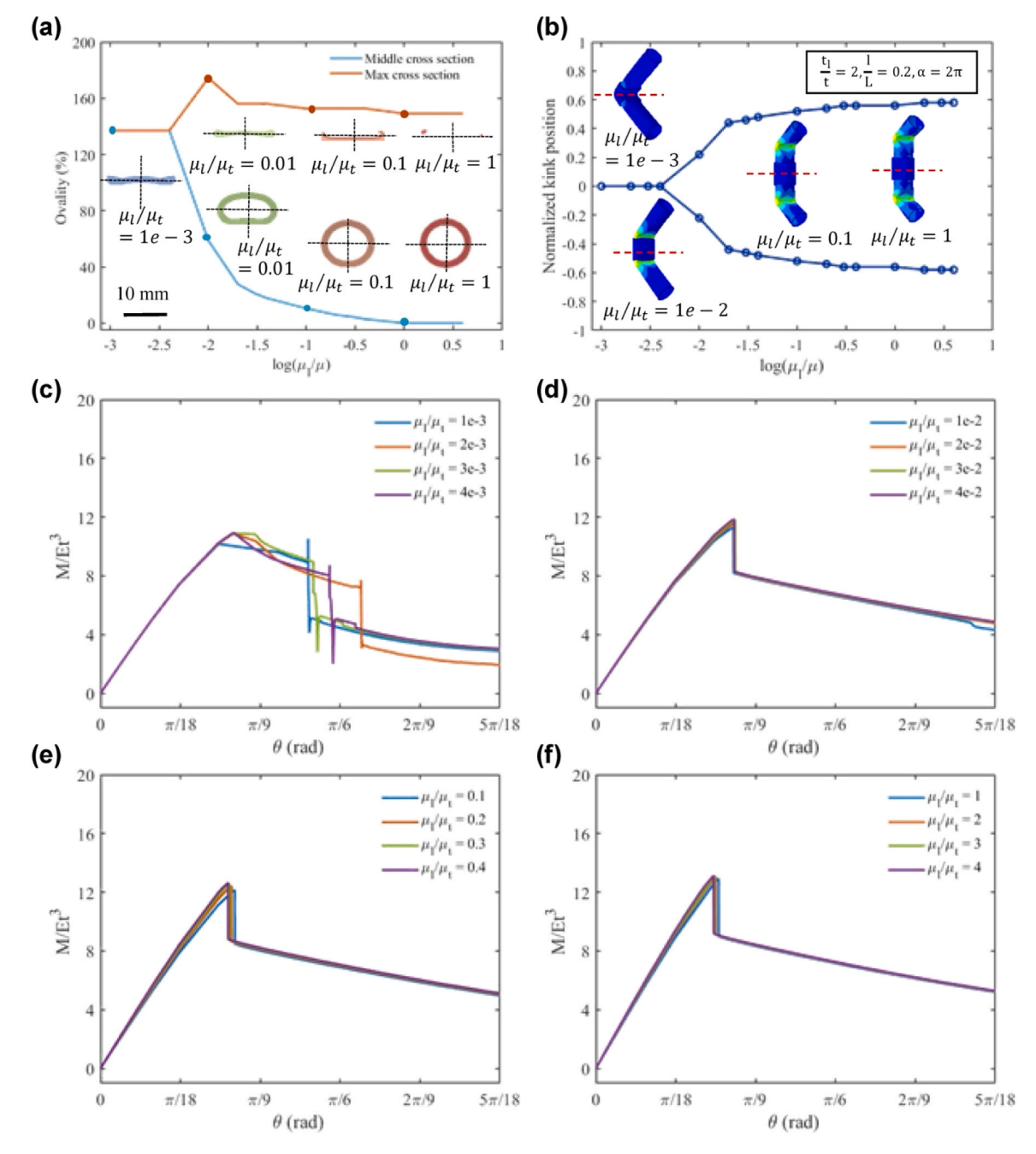


Fig. 6. Influence of relative stiffness between the sensor layer and the tube on ovalization and buckling behavior. (a) FEA results of ovality at a bending angle of $5\pi/18$ for various relative stiffness values (μ_l/μ_t). (b) Normalized kink position relative to the tube centerline. (c-f) FEA results of normalized moment-bending angle curves for different stiffness ranges: (c) $\mu_l/\mu_t = 1 \times 10^{-3} - 4 \times 10^{-3}$; (d) $\mu_l/\mu_t = 1 \times 10^{-2} - 4 \times 10^{-2}$; (e) $\mu_l/\mu_t = 0.1 - 0.4$; (f) $\mu_l/\mu_t = 1 - 4$.

- Order 10⁻³: Critical moments remain nearly constant across ratios, but the post-buckling response shows multiple deformation events, reflecting low stiffness influence.
- Order 10⁻²: A transition occurs (critical moment increases to 11.81)
 and buckling patterns become more spatially organized, with
 deformation shifting to uncovered zones.
- Order 10⁻¹: Further increases in stiffness yield a critical moment of 12.63, and consistent wrinkle formation appears, reflecting stronger interfacial constraints.
- **Order** 10⁰: The highest critical moment (13.12) is observed. Buckling occurs earlier and predominantly outside the stiffened region, with stable post-buckling characteristics.

These results reveal a contrast-driven preferential buckling mechanism, where stiffness mismatch redistributes global strain energy and drives instability into more compliant, uncovered regions. As the sensor layer becomes stiffer, it effectively suppresses local deformation, elevates load-bearing capacity, and stabilizes post-buckling behavior in the covered region. However, this benefit comes at the cost of concentrating stresses in unreinforced areas. This mechanism extends classical theories of tube instability—such as Brazier's model—by incorporating nonlinear hyperelastic layering effects that promote multi-stage buckling through progressive stiffness loss and wrinkle formation [8]. The findings emphasize that stiffness ratios exceeding 0.03 are critical for suppressing mid-plane ovalization and enhancing the structural performance of soft hybrid systems. In smart infrastructure applications-such as pipelines exposed to vibration, wind-induced bridge flexure, or bending in embedded sensor networks-strategically designed stiffness ratios improve sensor layer integrity, reduce risks of delamination, and ensure long-term sensing reliability under operational loading.

5. Conclusion

This study systematically investigated the mechanics of bonded sensor layers in mitigating bending-induced ovalization, buckling, and layer failure in soft, thin-walled tubular structures, with the aim of enhancing sensing reliability under operational conditions. Through integrated finite element analysis and experimental validation, we demonstrated that key parameters-including length ratio, thickness ratio, wrapped angle, and relative stiffness-govern the onset and evolution of structural instability. Optimized configurations, such as length ratios exceeding 0.7, thickness ratios above 1.6, wrapped angles in the range of approximately $2\pi/3$ to $4\pi/3$, and relative stiffness values greater than 0.03, were found to suppress ovalization to below 25 % in the covered regions. These configurations also redistributed deformation to the uncovered areas, leading to complex buckling behaviors involving multiple kinks and secondary post-buckling events. Such mechanisms reduce strain concentrations, mitigate the risks of sensor wrinkling or delamination, and help preserve measurement fidelity in embedded sensing systems. The new findings advance the understanding of layered hyperelastic interactions in soft tubular systems, extending classical theories such as Brazier's to include the effects of circumferentially and axially heterogeneous stiffness distributions. The results provide a foundation for the design and integration of sensorized soft tubes in smart infrastructure applications, including structural health monitoring pipelines and environmental sensing networks. To further improve the predictive accuracy and practical relevance of the models, future research should incorporate factors such as internal pressure loading, cyclic fatigue, viscoelastic behavior, and imperfect bonding conditions.

CRediT authorship contribution statement

Yi Jin: Writing – original draft, Visualization, Validation, Methodology, Investigation, Formal analysis. Christian A. Zorman: Writing –

review & editing, Resources, Funding acquisition. **C. Chase Cao:** Writing – review & editing, Supervision, Resources, Methodology, Funding acquisition, Conceptualization.

Declaration of Competing Interest

The authors declare that they have no known competing financial interests or personal relationships that could have appeared to influence the work reported in this paper.

Acknowledgments

This work is partially supported by the National Science Foundation (ECCS-2024649), USDA NIFA (2021-67021-42113), Swagelok Company, and Case Western Reserve University.

Appendix A. Supporting information

Supplementary data associated with this article can be found in the online version at doi:10.1016/j.eml.2025.102405.

Data availability

No data was used for the research described in the article.

References

- R. Mehmood, S.S.I. Katib, I. Chlamtac, Smart Infrastructure and Applications, Springer, 2020.
- [2] C. Talamo, et al., Smart cities and enabling technologies: influences on urban facility management services, in: IOP Conference Series: Earth and Environmental Science, IOP Publishing, 2019.
- [3] S.B. Abdelkarim, et al., Urban facility management improving livability through smart public spaces in smart sustainable cities, Sustainability 15 (23) (2023) 16257
- [4] M.D.Y. Moussa, et al., Smart pipeline monitoring system: a review, in: 2023 International Conference on Energy, Power, Environment, Control, and Computing (ICEPECC), IEEE, 2023.
- [5] Q. Zhao, et al., Novel integrated optical fiber sensor for temperature, pressure and flow measurement, Sens. Actuators A: Phys. 280 (2018) 68–75.
- [6] H. Cunfu, et al., Theoretical and experimental studies of torsion deformation of athin-walled tube with wound and pasted shape memory alloy wires, Smart Mater. Struct. 9 (5) (2000) 660.
- [7] S. Houliara, S. Karamanos, Buckling and post-buckling of long pressurized elastic thin-walled tubes under in-plane bending, Int. J. Non-Linear Mech. 41 (4) (2006) 491–511.
- [8] On the flexure of thin cylindrical shells and other "thin" sections, Proc. R. Soc. Lond. Ser. A Contain. Pap. Math. Phys. Charact., vol. 116(no. 773) 1927.
- [9] Y. Liu, E. D, Effects of cross-sectional ovalization on springback and strain distribution of circular tubes under bending, J. Mater. Eng. Perform. 20 (9) (2011) 1591–1599.
- [10] Q. Lei, et al., On the pressure-torsion response of a flexible pipe with section ovalization, Appl. Ocean Res. 127 (2022) 103297.
- [11] C. Iandiorio, P. Salvini, Bending ovalization of thin-walled circular tubes, Adv. Sci. Technol. 144 (2024) 135–150.
- [12] Mark Runciman, Darzi Ara, P. M, Soft robotics in minimally invasive surgery, Soft Robot. 6 (4) (2019).
- [13] G. Blewitt, et al., A review of worm-like pipe inspection robots: research, trends and challenges, Soft Sci. 4 (2) (2024) 13.
- [14] G.A.A.V. Luna, et al., A review on soft in-pipe navigation robot from the perspective of material, structure, locomotion strategy, and actuation technique | Robotica | Cambridge Core, Robotica 43 (1) (2025).
- [15] M, K, Z. Y, J. S, Soft tissue surgical robot for minimally invasive surgery: a review PubMed, Biomed. Eng. Lett. 13 (4) (2023).
- [16] S. Chen, et al., Soft robotic manipulation system capable of stiffness variation and dexterous operation for safe human–machine interactions, Adv. Mater. Technol. 6 (5) (2021) 2100084.
- [17] Zhao Y., et al., Self-adaptive, untethered soft gripper system for efficient agricultural harvesting, J. Field Robot., vol. $n/a(no.\ n/a)$.
- [18] X. Liu, et al., Soft humanoid hands with large grasping force enabled by flexible hybrid pneumatic actuators, Soft Robot. 8 (2) (2020) 175–185.
- [19] X. Liu, et al., Worm-Inspired soft robots enable adaptable pipeline and tunnel inspection, Adv. Intell. Syst. 4 (1) (2022) 2100128.
- [20] C. Iandiorio, P. Salvini, Bending ovalization of thin-walled circular tubes Scientific.Net, Adv. Sci. Technol. (2024) 144.
- [21] S.V. Levyakov, S.V. Levyakov, Equations of finite bending of thin-walled curvilinear tubes, J. Appl. Mech. Tech. Phys. 42 (5) (2001).

- [22] O. Fabian, Collapse of cylindrical, elastic tubes under combined bending, pressure and axial loads, Int. J. Solids Struct. 13 (12) (1977).
- [23] W.B. Stephens, J.H.S. Jr, B.O. Almroth, Collapse of long cylindrical shells under combined bending and pressure loads, AIAA J. 13 (1) (2012).
- [24] S.A. Karamanos, et al., Tubular members. I: stability analysis and preliminary results, J. Eng. Mech. 122 (1) (1996).
- [25] A.K. Habtemariam, et al., Generalized beam theory formulation for thin-walled pipes with circular axis, Thin-Walled Struct. 159 (2021).
- [26] D. Mazor, O. Rand, The influence of the in-plane warping on the behavior of thin-walled beams, Thin-Walled Struct. 37 (4) (2000).
- [27] E. Corona, S. Kyriakides, An experimental investigation of the degradation and buckling of circular tubes under cyclic bending and external pressure, Thin-Walled Struct. 12 (3) (1991).
- [28] M. Ju, et al., Numerical simulations and experimental study on the reeling process of submarine pipeline by R-Lay method, J. Mar. Sci. Eng. 9 (6) (2021) 579.
- [29] E.W. WILKES, On the stability of a circular tube under end thrust, Q. J. Mech. Appl. Math. 8 (1) (1955).
- [30] L.C. Zhang, T.X. Yu, An investigation of the brazier effect of a cylindrical tube under pure elastic-plastic bending, Int. J. Press. Vessels Pip. 30 (2) (1987).
- [31] Z. Zhang, Z. Zhang, Finite element simulation study on residual cross-sectional ovalization of thin-walled circular steel tubes in continuous rotary straightening process, Int. J. Adv. Manuf. Technol. 102 (5) (2019).
- [32] Z. Zhang, Modeling and simulation for cross-sectional ovalization of thin-walled tubes in continuous rotary straightening process, Int. J. Mech. Sci. (2019) 153–154.
- [33] K. Park, G.H. Paulino, Cohesive zone models: a critical review of tractionseparation relationships across fracture surfaces, Appl. Mech. Rev. 64 (6) (2011) 060802